

# Target tracking and pointing for arrays of phase-locked lasers

Van P. Macasaet<sup>a</sup>, Gary B. Hughes<sup>b</sup>, Philip Lubin<sup>c</sup>, Jonathan Madajian<sup>c</sup>, Qicheng Zhang<sup>c</sup>, Janelle Griswold<sup>c</sup>, Neeraj Kulkarni<sup>c</sup>, Alexander Cohen<sup>b</sup>, and Travis Brashears<sup>c</sup>

[gbhughes@calpoly.edu](mailto:gbhughes@calpoly.edu)

[lubin@deepspace.ucsb.edu](mailto:lubin@deepspace.ucsb.edu)

<sup>a</sup>Aerospace Engineering Department, California Polytechnic State University, San Luis Obispo, CA 93407-0405

<sup>b</sup>Statistics Department, California Polytechnic State University, San Luis Obispo, CA 93407-0405

<sup>c</sup>Physics Department, University of California, Santa Barbara, CA 93106-9530

## ABSTRACT

Arrays of phase-locked lasers are envisioned for planetary defense and exploration systems. High-energy beams focused on a threatening asteroid evaporate surface material, creating a reactionary thrust that alters the asteroid's orbit. The same system could be used to probe an asteroid's composition, to search for unknown asteroids, and to propel interplanetary and interstellar spacecraft. Phased-array designs are capable of producing high beam intensity, and allow beam steering and beam profile manipulation. Modular designs allow ongoing addition of emitter elements to a growing array. This paper discusses pointing control for extensible laser arrays. Rough pointing is determined by spacecraft attitude control. Lateral movement of the laser emitter tips behind the optical elements provides intermediate pointing adjustment for individual array elements and beam steering. Precision beam steering and beam formation is accomplished by coordinated phase modulation across the array. Added cells are incorporated into the phase control scheme by precise alignment to local mechanical datums using fast, optical relative position sensors. Infrared target sensors are also positioned within the datum scheme, and provide information about the target vector relative to datum coordinates at each emitter. Multiple target sensors allow refined determination of the target normal plane, providing information to the phase controller for each emitter. As emitters and sensors are added, local position data allows accurate prediction of the relative global position of emitters across the array, providing additional constraints to the phase controllers. Mechanical design and associated phase control that is scalable for target distance and number of emitters is presented.

### Keywords:

DE-STAR, Directed Energy, Planetary Defense, Laser Array Design

## 1. INTRODUCTION

### 1.1. Directed Energy for Planetary Defense and Solar System Exploration

Directed energy has recently been investigated as an enabling technology for many planetary science missions, including asteroid orbit alteration,<sup>1-7</sup> asteroid composition analysis,<sup>8</sup> near-Earth object (NEO) search,<sup>9</sup> beamed propulsion,<sup>10,11</sup> and more. The space-based laser systems envisioned in these studies consist of a planar array of coherently-combined laser emitters using fiber amplifiers and associated optical elements, powered by photovoltaics. Small arrays would be useful for missions that deploy to an area near the asteroid. Larger arrays would be capable of operating from large distances, allowing consideration of an Earth-orbiting system. In order to form and steer a concentrated directed-energy beam, precise relative phase control over the entire array of lasers is required. Such phase control requires attention to several key aspects of system design that can affect the relative phases of every emitter, including: (1) mechanical alignment of laser and optical components; (2) structural vibration; (3) reference phase generation and acquisition; (4) electronic and/or mechanical emitter phase control. This paper describes an overall approach for targeting, pointing and phase control for beam formation and steering in an array of coherently-combined laser emitters.

### 1.2. Local Control for an Array of Phase-Locked Lasers

The current vision for laser arrays is based on fiber amplifier technology.<sup>12-17</sup> Laser fiber amplifiers emit very narrow-band energy beams at a wavelength of 1.06  $\mu\text{m}$ . Individual elements of the array are modest power (kW class each) amplifiers that are phase-controllable for beam formation and steering. Baseline technology has been developed in the laboratory, and deployed in field systems.

A common approach for phase control uses a Stochastic Parallel Gradient Descent (SPGD) algorithm.<sup>18-21</sup> The SPGD control scheme employs a beamsplitter to sample the outgoing phase of each individual emitter (Fig. 1). The design requires the beamsplitter to be optically flat over the combined aperture of the overall array. Alternatively, structural aberrations in the beamsplitter could be characterized during a calibration procedure, and compensations could be implemented in the controller. Such a calibration procedure is capable of compensating for static anomalies in the beamsplitter. It may also be possible for the controller to compensate for some transient aberrations that mutate more slowly than the minimum control response time. These disadvantages are tenable when the objective is to build an array with a fixed number of emitters. That is, careful construction of the array and programming of the controller can readily compensate for optical imperfections in system components. Stand-on missions could be designed around a fixed-sized array, using current phased array designs.

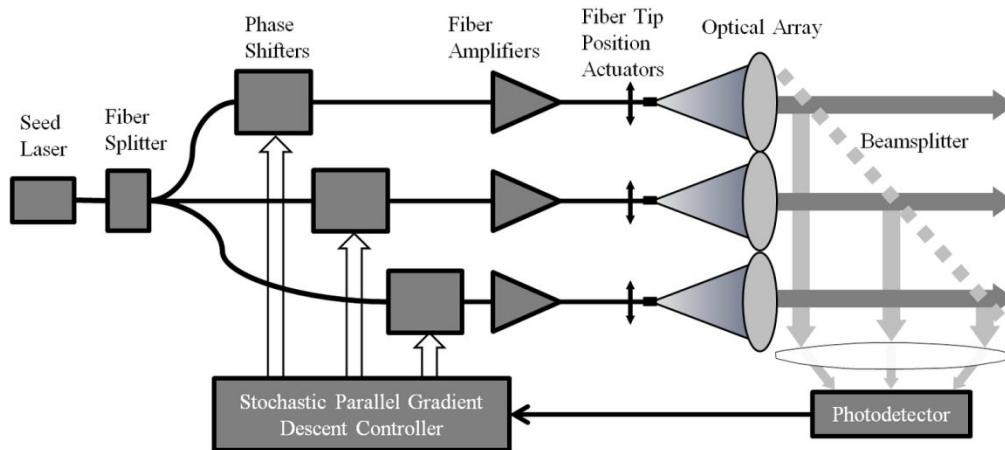


**Figure 1.** Stochastic Parallel Gradient Descent (SPGD) control scheme used in existing laser phased array laser systems, based on high-power laser fiber amplifiers. Existing phased array designs rely on the flatness of the beamsplitter to provide relative phase control.

### 1.3. Modular Design for Extensible Phase-Locked Array

The SPGD scheme is not extensible, in so far as adding additional laser elements to the array would require installation of a larger beamsplitter. Based on current designs, if an emitter were added to the array, the beamsplitter would need to be expanded to cover the new array aperture. Replacing an existing beamsplitter with a larger one, or adding a segment to an existing beamsplitter, to cover the additional emitter would require a re-calibration of the added emitter to the rest of the array. In the context of an orbiting platform, re-calibration of the control components is impractical.

A baseline design for extensible array is shown in Fig. 2. The beamsplitter function is replaced by a reference source in front of the array, and fast, high-precision structural metrology. A seed laser supplies a reference source for the array of fiber amplifiers. Rough pointing of the array to the target is determined by spacecraft attitude control. Fiber tips behind each optical element are mounted to micro-positioner actuators; lateral movement of the laser tips behind each lens provides intermediate pointing adjustment for individual array elements and beam steering. Precision beam steering and beam formation (spot focus) is accomplished by coordinated phase modulation across the array. Feedback from wavefront sensors in front of the optical elements is used to adjust the input phase to each amplifier. This scheme requires a phase reference signal to be present at the exit aperture of each optical element. Ideally, the reference signal would consist of parallel wavefronts travelling along the target axis. Geometric constraints require novel approaches to generation and use of the phase reference signal.

The phased array design and control scheme employs hexagonal emitter cell units that include a phase tap structure. Unit cells are built and calibrated in the factory, and the modular design supports mechanical attachment of additional emitter cells to an existing array, without the need to modify or re-calibrate any aspect of existing emitter components. As an emitter is added to an existing array, the control module input/output (I/O) configuration is updated to accommodate the additional sensors and controls. The phase perturbations in individual beams that must be counteracted, namely fast structural vibration and slow thermal drift, can be measured and corrected for with electronic phase control in the fiber amplifier chain. A local control scheme is independent of target and range and is more easily scalable in both

power and array size. Structural vibrations may have large enough amplitudes to deflect the beam away from the target. In addition, the structure of each beam's cell has been optimized to reduce structural modes as much as possible.

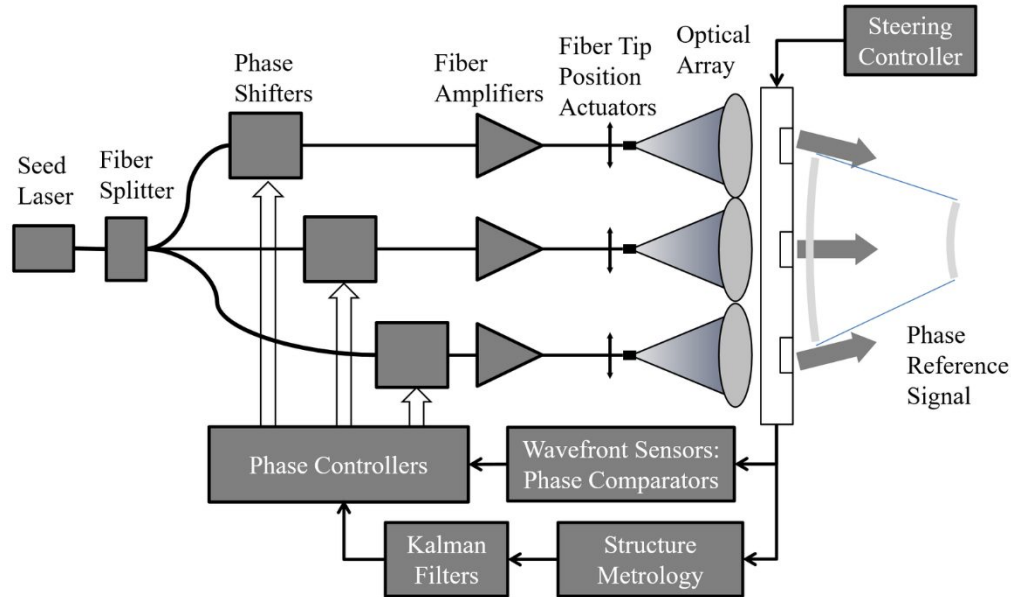


**Figure 2.** Concept for extensible phased array design. The combination of a phase reference signal, such as a reflector, and structural metrology provide a mechanism for relative phase control.

The core idea of the new design is that the relative phases of adjacent beams are determined with respect to a target plane. The relative position between adjacent phase sensors is determined with respect to a mechanical datum that is located at the center of a target sensor. Calibration of individual emitters is accomplished during module assembly, and calibration data is added to the array controller. The conceptual design of Fig. 2 can be implemented as an array of individual hexagonal emitters, as shown in Fig. 3 and Fig. 4. A phase tap structure is situated between adjacent pairs of emitters. The phase tap includes a target sensor, shown in Fig. 3 as dark circles. When a single target sensor is present, the direction of the target can be derived from the datum coordinate system of the sensor focal plane. When more than one target sensor is present, the target direction can be determined from a combination of the individual direction vectors. In order to combine two or more target vectors, the relative position of the local datum coordinate systems must be determined. The phase tap structures are equipped with six degree-of-freedom relative position sensors that provide fast, high precision relative position sensing.<sup>22</sup> The mechanical design and phase control concept are illustrated in Fig. 5 and Fig. 6. The relative position sensor is described in §2.

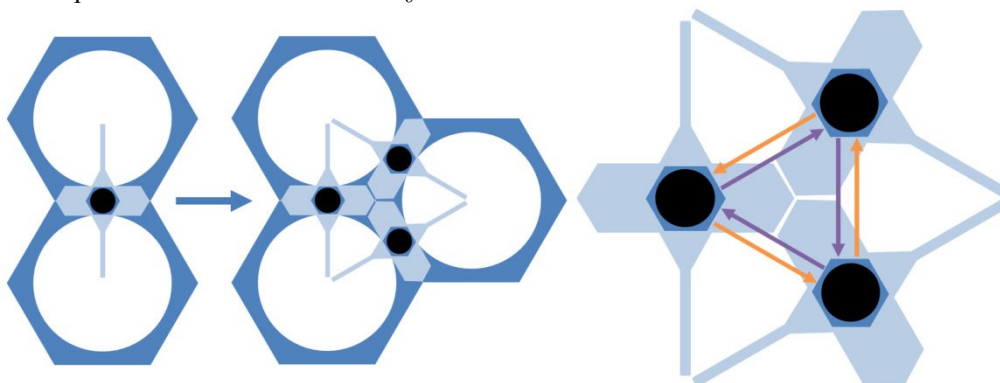


**Figure 3.** Conceptual diagram of three adjacent cells of a laser phased array. Three phase tap structures are used to connect the adjacent cells. The relative position between adjacent phase tap structures is determined with 2D-AFM position sensors (shown in Fig. 5 and Fig. 6).

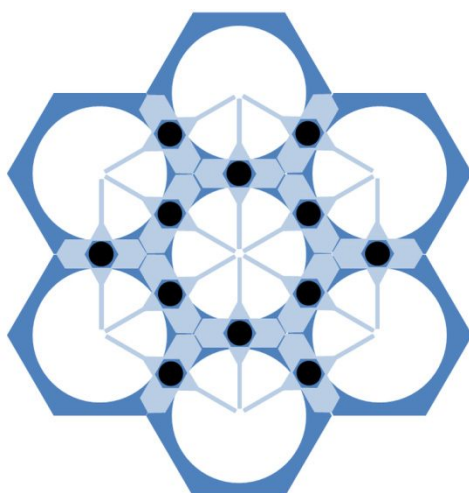


**Figure 4.** Conceptual diagram of three adjacent cells of a laser phased array. Three phase tap structures are used to connect the adjacent cells. The relative position between adjacent phase tap structures is determined with 2D-AFM position sensors (shown in Fig. 5).

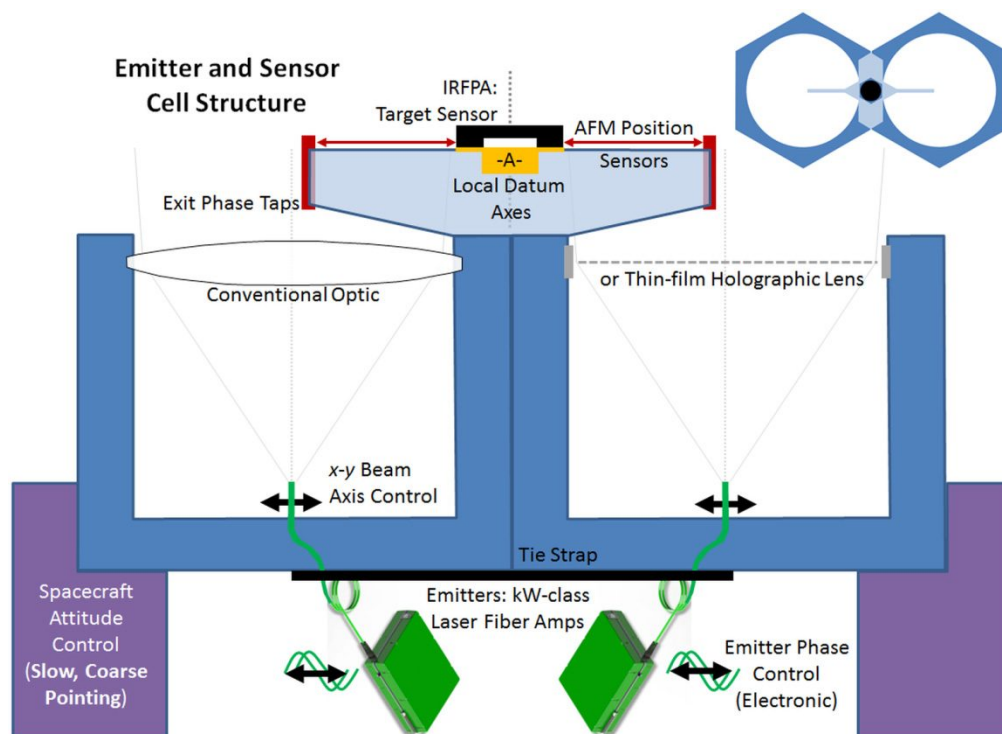


**Figure 5.** Conceptual diagram of a 2-element laser phased array architecture. A single phase tap structure connects the two emitter cells. Datum -A- is a mechanical reference location that provides a common coordinate system for the target vector and the phase control mechanism. Mission parameters drive the optical configuration. For a stand-on mission, such as DE-STARLITE, an example might be to seek a 1 m beam on a target that is 10 km distant, leading to individual emitter lenses that are ~55 mm diameter.

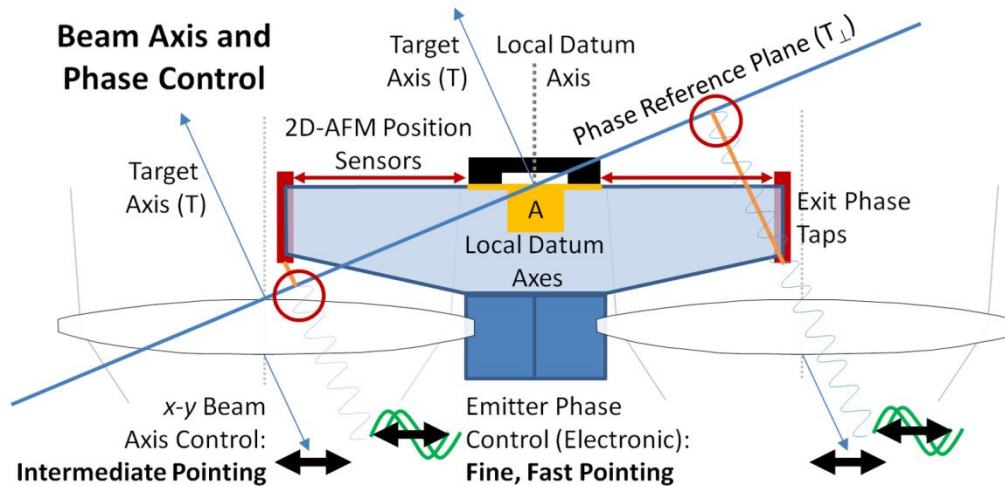


**Figure 6.** Conceptual diagram of a phase tap structure illustrating the mechanism for sensing the phase of individual elements in relation to the phase reference plane. The phase reference plane is derived from the target vector, using camera and sensor calibration information. The position of each exit phase tap in the mechanical datum coordinate system is measured with 2D-AFM position sensors. The calculated distance from the phase tap to the reference plane along the target vector provides the reference phase for aligning the two emitter phases.

#### 1.4. Beam Intensity Models and Estimation of Mechanical Alignment Requirements

A model is presented for beam formation by a coherently-combined laser array, based on previous work.<sup>23</sup> Beam intensity models are used to determine the relative phase alignment requirements for elements across the array. The model is suitable for estimating far-field beam intensity, under some assumptions about the source of phase mis-alignment in a coherently-combined laser array. The interference pattern and resulting far-field intensity distribution of multiple emitters in a phased-array design can be determined by scalar diffraction theory. The complex far-field amplitude for a linear array of emitters with static ( $E_f$ ) and time-varying ( $E_t$ ) phase misalignments at each emitter is given by:

$$E(\theta, t) = \frac{e^{[i \cdot k \cdot a \cdot \sin(\theta)]} - 1}{i \cdot k \cdot \sin(\theta)} \cdot \sum_{p=0}^{N-1} e^{i\{[k \cdot p \cdot d \cdot \sin(\theta) + E_f(p) + E_t(p, t)]\}} \quad (1)$$

Given the complex amplitude, the far-field beam intensity for the linear array is then:

$$I(\theta) = |E(\theta)|^2 \quad (2)$$

For a 1-D linear array, the far-field beam intensity for a square array with beam intensity  $I_x(\theta)$  along one axis and  $I_y(\psi)$  along a perpendicular axis is:

$$I(\theta, \psi) = I_x(\theta) \cdot I_y(\psi) \quad (3)$$

The simulation results shown in Fig. 7 represent a laser phased array far field intensity, based on Eq. (1)-(3). A simulation was run without phase perturbations. Simulations were also run that include fixed phase mis-alignments ( $E_f$ ) at each emitter with a  $1\sigma$  error of  $\lambda/8$ . Comparison of the two simulations shows significant beam degradation, with power moving from the main peak to side lobes. Also evident from the simulation results is a pointing shift, *i.e.*, the main lobe axis is no longer aligned with the array axis, with a pointing error on the order of  $1 \mu\text{rad}$ .

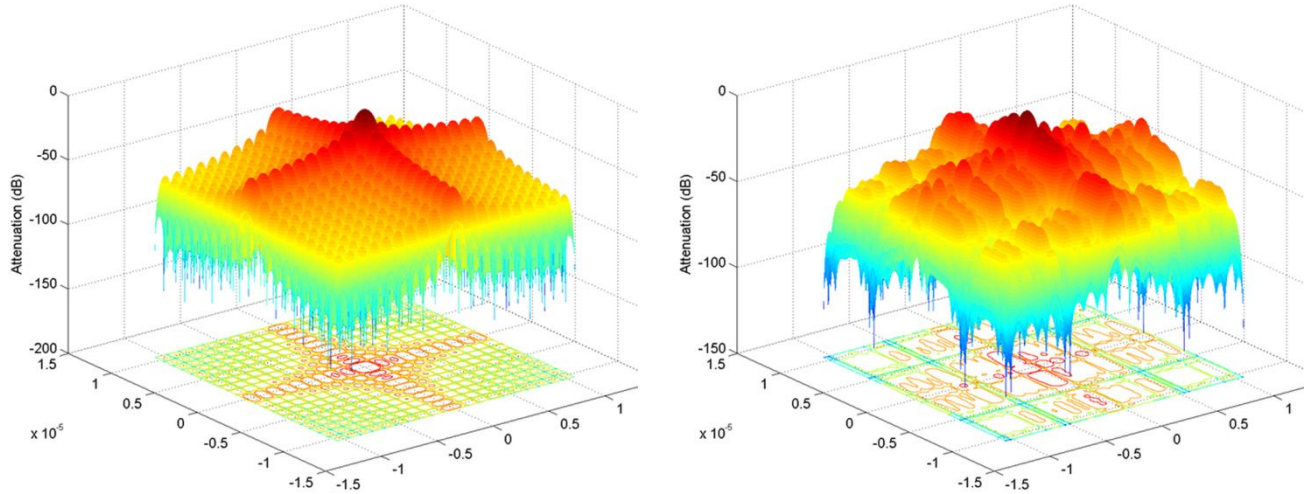


**Figure 7.** Simulation results for a 5 by 5 close-packed array of emitters, showing far-field intensity. Emitters are modeled as a close-packed array with 20 cm pitch, total aperture is 1 m, and the nominal emitter frequency is  $1.06 \mu\text{m}$ . **Left:** No phase perturbations. **Right:** Static phase perturbations due to mechanical mis-alignments were randomly assigned to each emitter, with magnitudes drawn from a normal distribution with  $1\sigma = 2\pi/8$ .

**Table 1.** Terms used in Eq. (1-3).

Symbol	Interpretation	Units
$I$	Time averaged intensity of beam	W/m
$c$	Speed of light in a vacuum	m/s
$\epsilon_0$	Permittivity of free space	F/m
$E_0$	Initial beam amplitude	N/C
$w_0$	Beam waist	m
$z$	Forward propagation distance	m
$r$	Radial propagation distance	m
$w(z)$	Spot size	m
$k$	Wave number	$\text{m}^{-1}$
$q(z)$	Complex radius of curvature	m
$R(z)$	Radius of curvature	m
$\omega$	Radial frequency	Hz
$t$	Time	s

**Table 2.** Phase Perturbation Terms

Type of Perturbation	Simulation Method	Real-World Analog
Optical Axis Deflection	A rotational matrix transformation is applied.	First and second mode vibrations of the structure.
Optical Axis Correction (large amplitude)	A rotational matrix is applied opposite to that above and lagging behind to simulate imperfect corrections.	Micropositioners inside the cell cavity.
Non-mechanical phase drift ( <i>i.e.</i> thermal, <i>etc.</i> )	A complex exponential with small amplitude and slow phase is multiplied by the wavefront.	Thermal fluctuations and other random phase disturbances.
Phase Drift and Small Amplitude Optical Axis Correction	A complex exponential with small amplitude fast phase is multiplied by the wavefront	Electronic phase control in fiber amplifiers.

## 2. A DYNAMIC RELATIVE POSITION SENSOR CONCEPT

### 2.1. Dynamic Metrology

The use of optoelectronic methods for dimensional metrology has many advantages, particularly when compared to mechanical methods. Optoelectronic measuring systems can acquire more data in less time and without contacting the measured object. Mechanical measuring systems can be prone to significant errors and deformities due to rapid wear.<sup>24-27</sup> Linear encoders with optical grating scales are the most common optoelectronic measuring devices used for high-precision applications. Simple optical encoder systems are based on the geometrical effect of phase-shifted optical relays for the conversion of the grating displacement relative to the read head into an electrical signal.<sup>28</sup> Linear encoders tend to be robust, even under unstable environmental conditions.

Since the invention of the helium-neon laser, in 1960, lasers have been used as coherent light sources for laser interferometry measurement systems. Optical laser interferometry is often used for displacement measurement applications that require high accuracy. Laser interferometers use a scale length of a well-defined wavelength and link it to the meter by frequency comparison definition. Homodyne sensors use two waves with the same wavelength that are phase shifted by 90 degrees and generated by polarization optics to determine the direction of motion and two additional signals with opposite phase are used to correct changes in the optical intensity. Heterodyne sensors compare slightly different frequencies with a reference beam, allowing the beat frequency of the interference signal to be detected. The phase of the beat frequency changes with the motion of the mirrors and can then be compared with a fixed reference frequency.

Triangulation sensors are often used for in-process metrology and coordinate metrology. Triangulation sensors exploit a collimated light source, generally a laser diode, and a detector unit. The detector unit consists of an imaging lens and a position-sensitive detector.<sup>29</sup> The optical axes of the imaging lens with the light source form a fixed angle. The surface of the object is brought close to the axes point of intersection and the diffused reflection of light is imaged onto the detector. Typical measurement ranges for triangulation systems are 2 m to 200 mm and can provide relative position measurements with resolutions in the range of  $10^{-4}$  m.

Dynamic metrology is concerned with the measurement of quantities that are time-dependent.<sup>30-50</sup> As the characteristics of interest are changing through time, methods of time series analysis have been employed to provide point estimate and uncertainty evolution based on data acquisition through time. Dynamic structural metrology, for instance, is concerned with how the relative position of components in a structure changes through time, as the structure flexes with temperature changes and vibrates in structural modes. Such technology has been developed for atomic force microscopes (AFMs). In an AFM, a molecular tip is mounted on the free end of a cantilever. As the tip is moved across the surface of a sample, molecular-scale movements of the cantilever are induced. A laser is reflected off the back side of the cantilever, and detected at a split photodiode. Movements of the cantilever are detected in the changing position of the laser spot on the photodiode. The AFM cantilever provides a ~3-DOF measurement system (although typical AFM systems only sense one or perhaps two of the potential movements). The AFM tip is typically a flat surface, and the single reflected laser spot moves across the photodiode. In a modification of AFM technology, 6-DOF measurement of the tip position could be attained by using an array of lasers, and by including a curved reflective surface such as a pyramid or hyperbolic paraboloid. The multiple reflected spots would be sensed, and changes in the relative position of the emitter component and reflective surface will shift the location of the reflected spots. Various motions produce independent shifts in the reflected spot locations, allowing full 6-DOF relative position determination. This paper describes an implementation of such a 6-DOF sensor. The sensors are illustrated as part of a system to correct for mechanical flexing of a structure with multiple target acquisition sensors. The sensors are envisioned to make control-time measurements of the relative position of sensor housings within a local mechanical datum coordinate system, thus improving the target vector from the sensing structure.

### 2.2. Sensor Concept

A sensor is envisioned to make dynamic measurements of the relative position of two components. The method uses an array of several laser emitters mounted on one component. The lasers are directed at a reflective surface on the second component. The reflective surface consists of a piecewise-planar pattern such as a pyramid, or more generally a curved reflective surface such as a hyperbolic paraboloid. The reflected spots are sensed at 2-dimensional photodiode arrays on the emitter component. Changes in the relative position of the emitter component and reflective surface will shift the location of the reflected spots within photodiode arrays. Relative motion in any degree of freedom produces

independent shifts in the reflected spot locations, allowing full 6-DOF relative position determination between the two component positions. Response time of the sensor is limited by the read-out rate of the photodiode arrays.

In one implementation, consider a series of parallel laser emitters mounted on the first component. Such an arrangement can be thought of as originating from a grid pattern in a fixed ‘emitter plane’ that is normal to the beam vector. A series of photodiode array detectors might be positioned at appropriate places within the emitter plane. Positions of each detector in the emitter plane depend on properties of the reflective surface, which is mounted on the second component. Many implementations are possible; the results presented in this paper are based on parallel emitters, with a suitable pattern of detectors in an emitter plane on the first component. The reflected beam locations in the emitter plane depend on the relative position of the two components. Geometric ray-tracing of the beam paths from the emitter plane (on the first component) to the reflective surface (on the second component) and back to the detectors (on the first component) provides a forward transformation that can predict the detected beam pattern for any relative alignment of the two components. Inversion of the forward transformation can be used to determine the relative alignment of the two components from a specific (measured) beam pattern. Transformations are described below for a 3-panel pyramid reflector, and for a hyperbolic paraboloid.

### 2.3. Pyramid Reflector

Consider an arrangement with several parallel emitters and their associated detectors, all situated in a single ‘emitter plane’ on the first component. Given a (unit-length) emitter direction vector  $E = \langle E_1, E_2, E_3 \rangle$ , an implicit emitter plane equation is:

$$E \cdot (x, y, z) = d_E \quad (4)$$

The emitters can be represented by points  $P_i$  ( $i = 1, 2, \dots, n_E = \text{number of emitters}$ ) in the emitter plane, *e.g.*:

$$P_i = (P_{i1}, P_{i2}, P_{i3}), \text{ with } E \cdot P_i = d_E \text{ and } E \equiv \frac{(P_j - P_i) \times (P_k - P_i)}{\| \cdot \|} \quad (5)$$

The notation  $\| \cdot \|$  indicates the Euclidean norm of the expression in the numerator, forcing the resulting vector to be unit-length. A beam emanates from the  $i^{\text{th}}$  emitter at point  $P_i$  and follows the direction vector  $E$ , so the parametric form for each emitter beam as it leaves the emitter plane is:

$$P_i + t \cdot E, \quad t \in \mathbb{R}, \quad i = 1 \text{ to } n_E \quad (6)$$

A pyramid reflector is constructed on the second component, consisting of ‘panels’ that reflect the emitted beams back toward the first component. The ‘pyramid’ shape will constrain the plane orientations, in particular none of the panels will be parallel, so there will be a single point of intersection representing the ‘apex’ of the pyramid,  $A = \langle A_1, A_2, A_3 \rangle$ . Reflector panels have (unit-length) normal vectors  $R_i$  and the implicit plane equations are:

$$R_i = \langle R_{i1}, R_{i2}, R_{i3} \rangle, \text{ with } R_i \cdot (x, y, z) = R_i \cdot A, \quad i = 1 \text{ to } n_E \quad (7)$$

The number of panels in the pyramid does not necessarily need to equal the number of emitters, *e.g.*, two or more emitters could strike the same panel; so, the set  $\{R_i\}$  could contain repeated vectors, but a reflective plane must be defined for each emitter. The points  $Q_i$  where the  $i^{\text{th}}$  emitter strikes the  $i^{\text{th}}$  plane is then found by travelling a distance  $t_i$  from the emitter location  $P_i$  along the emitter direction vector  $E$ :

$$Q_i = P_i + t_i \cdot E \quad (8)$$

The distance  $t_i$  can be determined directly, since  $Q_i$  lies in the reflector panel plane<sup>49</sup>, *i.e.*, from Eq. (4):

$$R_i \cdot Q_i = R_i \cdot A \quad (9)$$

Substitute the expression for  $Q_i$  from Eq. (5) into Eq. (6):

$$R_i \cdot (P_i + t_i \cdot E) = R_i \cdot A \quad (10)$$

Distribute the inner product across the sum in Eq. (7) to solve for  $t_i$ :

$$t_i = \frac{R_i \cdot (A - P_i)}{R_i \cdot E} \quad (11)$$

The points  $Q_i$  are then found by:

$$Q_i = P_i + \left( \frac{R_i \cdot (A - P_i)}{R_i \cdot E} \right) \cdot E \quad (12)$$

Assuming specular reflection, the  $i^{\text{th}}$  incident beam will be reflected across the panel normal  $R_i$  at the point  $Q_i$ . The reflected beam will lie in a ‘reflection plane’ containing the point  $Q_i$ . A (unit) vector  $N_i$  that is normal to the reflection plane can be determined by the cross product of the incident beam vector  $E$  and the panel normal vector  $R_i$ :

$$N_i = \langle N_{i1}, N_{i2}, N_{i3} \rangle = \frac{E \times R_i}{\| \cdot \|} \quad (13)$$

The incident angle is between  $E$  and  $R_i$  (which are both unit length):

$$\theta_i = \text{acos}(E \cdot R_i) \quad (14)$$

The reflected beam emanates from  $Q_i$ , at an angle  $2\theta_i$  from  $E$  around the axis of rotation  $N_i$ . A (unit) vector  $S_i$  in the direction of the reflected light is determined by rotating the incident beam (unit) vector in the rotation plane, *i.e.*, around the rotation vector  $N_i$ , by an angle  $2\theta$ <sup>49</sup>:

$$S_i = \frac{M_i \cdot E}{\| \cdot \|} \quad (15)$$

$$M_i = \begin{bmatrix} \cos(2\theta_i) + N_{i1}^2[1 - \cos(2\theta_i)] & -N_{i3}\sin(2\theta_i) + N_{i1}N_{i2}[1 - \cos(2\theta_i)] & N_{i2}\sin(2\theta_i) + N_{i1}N_{i3}[1 - \cos(2\theta_i)] \\ N_{i3}\sin(2\theta_i) + N_{i1}N_{i2}[1 - \cos(2\theta_i)] & \cos(2\theta_i) + N_{i2}^2[1 - \cos(2\theta_i)] & -N_{i1}\sin(2\theta_i) + N_{i2}N_{i3}[1 - \cos(2\theta_i)] \\ -N_{i2}\sin(2\theta_i) + N_{i1}N_{i3}[1 - \cos(2\theta_i)] & N_{i1}\sin(2\theta_i) + N_{i2}N_{i3}[1 - \cos(2\theta_i)] & \cos(2\theta_i) + N_{i3}^2[1 - \cos(2\theta_i)] \end{bmatrix} \quad (16)$$

By the same process shown in Eq. (5) through Eq. (8), the points  $P'_i$  where the  $i^{\text{th}}$  reflected beam strikes the emitter plane are found by travelling a distance  $t'_i$  from the incident locations  $Q_i$  along the reflected direction vectors  $S_i$ . The distances  $t'_i$  are:

$$E \cdot P'_i = d_E \rightarrow E \cdot (Q_i + t'_i \cdot S_i) = d_E \rightarrow t'_i = \frac{d_E - E \cdot Q_i}{E \cdot S_i} \quad (17)$$

And the points  $P'_i$  are then found by:

$$P'_i = Q_i + t'_i \cdot S_i \quad (18)$$

Thus far, geometric ray traces from  $P_i$  to  $P'_i$  have been established as:

$$P'_i = P_i + \left( \frac{R_i \cdot (A - P_i)}{R_i \cdot E} \right) E + \left( \frac{d_E - E \cdot Q_i}{E \cdot S_i} \right) S_i \quad (19)$$

where  $S_i$  is defined in Eq. (15) and Eq. (16). The ray trace assumes that the emitters are all parallel and lie in a plane that is normal to the emitter beams, that the rays are sensed in the same emitter plane, and that the reflection is specular. A simulated reflector based on the pyramid reflector model is shown in Fig. 8.

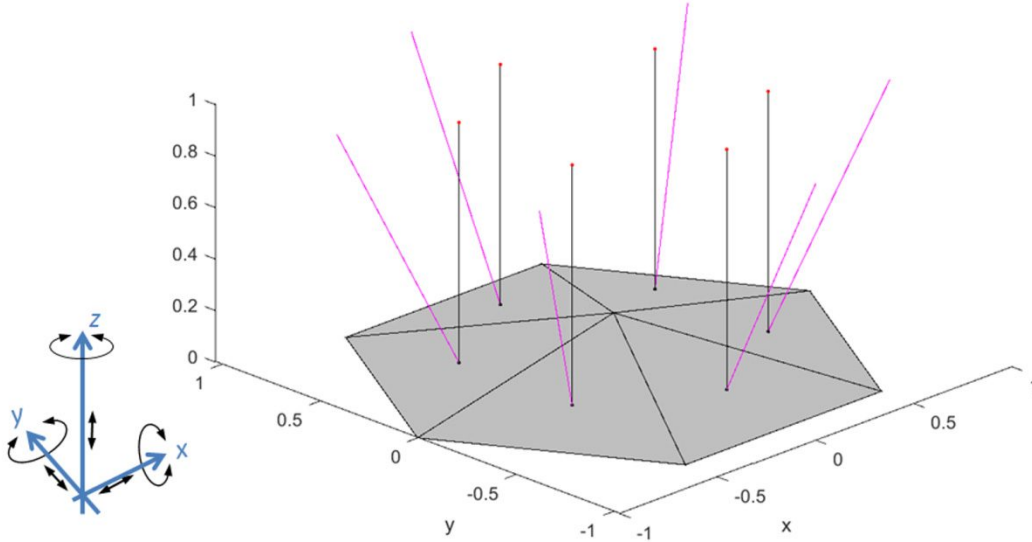


**Figure 8.** Conceptual diagram of a 6-DOF relative position measurement scheme, using a pyramid reflector. Laser emitters mounted on one component are directed at a reflective pyramid that is mounted on a second component. The reflected spots are sensed in separate 2-D photodiode arrays on the first component. Changes in the relative position of the emitter plane and reflective surface will shift the location of reflected spots. Kinematic and independent motions ensure that the measured spot locations can be used to determine the relative position of the emitter plane and the reflective surface. The implementation in this figure shows six parallel laser emitters emanating from a normal plane, where the detector arrays would also be mounted.

## 2.4. Relative Position from Reflected Spot Location Measurements

Relative motion of the reflective surface in any of the six degrees of freedom will result in a kinematic displacement of the reflected point  $P$ . For example, a translation in the  $z$ -axis ( $\Delta z \equiv \langle 0, 0, \Delta z \rangle$ , which occurs with thermal expansion), results in displacement of  $P$  that depends on the distance between the emitter plane and the reflective surface ( $d$ ), and curvature properties of the reflective surface (determined by  $a$  and  $b$ ):

$$\Delta P = (Q + \Delta z) + \frac{d-E \cdot (Q+\Delta z)}{E \cdot R} \cdot R \quad (20)$$

The change in location of the reflected spot  $P$  for a given change in the  $z$ -location of the reflective surface is kinematic. For example, for motions in the  $z$ -axis, the calculation for change in the reflected spot position is easily invertible:

$$\Delta P = (Q + \Delta z) + \frac{d-E \cdot (Q+\Delta z)}{E \cdot R} \cdot R \rightarrow \Delta z = \frac{(\Delta P - Q)(E \cdot R) - (d - E \cdot Q)R}{E \cdot R - E(3)} \quad (21)$$

Additionally, changes in the reflected multi-spot pattern are independent for motions in the six degrees of freedom when a pyramid, hyperbolic paraboloid or other curved surface is used as the reflecting component. Kinematic motions and independent changes in the spot pattern ensure that position determination is invertible for simultaneous motions in all degrees of freedom, *i.e.*, for some measured change in the spot location from the nominal  $\langle \Delta x, \Delta y, \Delta z, \Delta \theta_x, \Delta \theta_y, \Delta \theta_z \rangle$ , the relative position of the emitter plane and reflective plane can be determined. The forward ray tracing transformations provide a framework for constrained optimization calculations. Since the number of data points required for the optimization is small, the numerical inversion is fast enough to keep pace with dynamic measurements coming from the photodiodes.

## 2.5. Target Acquisition with Multiple Focal Planes

An application of the sensor concept is envisioned as part of a system to correct for mechanical flexing of a structure with multiple target acquisition sensors. The sensors are envisioned to make control-time measurements of the relative position of sensor housings within a local mechanical datum coordinate system, thus improving the target vector from the sensing structure. The target is viewed, for example using an infrared imaging system, consisting of an optic and an infrared focal plane array (IRFPA) that are mounted together in a mechanical housing. A conceptual drawing is shown in Fig. 3, based on a design for an extensible phased array laser system.<sup>51,52</sup> Target acquisition algorithms determine the target centroid  $\langle x_c, y_c \rangle$  in the IRFPA pixel array coordinate system. Using camera calibration information, the target centroid  $\langle x_c, y_c \rangle$  is then converted to a target axis  $\langle \theta_T, \varphi_T \rangle$  as polar ( $\theta$ ) and azimuthal ( $\varphi$ ) directions in the infrared camera mount mechanical datum coordinate system, using transformations deduced from innovative calibration algorithms.<sup>53-56</sup> Conversion from image coordinates to the target axis is accomplished using a composite inverse transformation.<sup>52</sup>

$$\begin{bmatrix} \theta_T \\ \varphi_T \end{bmatrix} = (A \circ D \circ F)^{-1} \begin{bmatrix} x_c \\ y_c \end{bmatrix} \quad (22)$$

where  $F$  is the transformation from the target axis to ideal pixel coordinates,  $D$  is a lens distortion mapping, and  $A$  is the ideal affine transformation from scene coordinates to pixel coordinates, all determined during camera calibration.

The relationship between pixel coordinates and the mechanical mounting is also characterized during fabrication. Precision machining is not adequate for ultra-precision alignment, but statistical calibration/characterization techniques are available. The statistical approach reduces measurement error and supports ultra-precision alignment with 'irregular' machined datum surfaces.

## 2.6. Pointing and Phase Alignment of a Laser Array

The system depicted in Fig. 3 shows a phased array laser system with multiple target acquisition sensors. The relative position of adjacent target sensors is determined using 6-DOF relative position sensors. The emitter plane maintains a rigid spatial relationship within the mechanical datum coordinate system, and the phase tap maintains a rigid spatial relationship to the reflective plane. Using the relative position of the reflective plane, and the rigid relationships, the position of the phase tap within the mechanical datum coordinate system is determined. The target axis  $\langle \theta_T, \varphi_T \rangle$  in the mechanical datum coordinate system is used to establish the target plane, which (arbitrarily) passes through the datum origin. The plane becomes the phase reference plane, which is:

$$N_T \cdot \langle x, y, z \rangle = 0, \quad N_T = \frac{\langle \cos(\theta_T)\sin(\varphi_T), \sin(\theta_T)\sin(\varphi_T), 1 \rangle}{\| \langle \cos(\theta_T)\sin(\varphi_T), \sin(\theta_T)\sin(\varphi_T), 1 \rangle \|} \quad (23)$$

A single phase tap structure connects two adjacent emitters. A nominal location of the phase taps within the mechanical datum coordinate system are determined during factory calibration. The target plane is the phase reference plane: the

control system must seek to align the phases of all emitters to the same value at the target plane. Deviations from the calibrated (mechanical datum) location of the phase taps are determined in control time with AFM relative position sensors. The distance of the phase taps from the phase reference plane can then be determined.

$$D_{ref} = \frac{N_T \cdot \langle x_{tap}, y_{tap}, z_{tap} \rangle}{\|N_T\|} = N_T \cdot \langle x_{tap}, y_{tap}, z_{tap} \rangle \quad (24)$$

Distance along the target vector from the phase tap provides the phase alignment target at the phase tap. Phase alignment is modulo one cycle, *e.g.*, shift the measured phase  $\phi_{meas}$  of an emitter to zero in the phase alignment plane:

$$\Delta\phi = \phi_{meas} - \frac{\frac{D_{ref}}{\lambda} - \lfloor \frac{D_{ref}}{\lambda} \rfloor}{2\pi} \quad (25)$$

### 2.7. Coarse, Intermediate and Precision Pointing, and Beam Steering

The preceding discussion of the emitter array architecture forms the basis for a phase feedback control scheme. In this paper, it is assumed that spacecraft attitude control ('rough pointing',  $\sim 10$  m rad in the example presented above) is adequate, and does not introduce significant pointing jitter into the target acquisition sensors. The 'rough pointing' control system operates independently from the 'intermediate pointing' (beam axis) and 'fine pointing' (beam steering) control systems. The intermediate and fine control systems are based on sensors consisting of phase taps, 6-DOF position sensors and target sensors. Control system actuators consist of *x-y* emitter positioners (or hexapods), and phase controllers. An array with *n* emitters has  $4n - 6$  phase taps,  $2n - 3$  IRFPA target sensors, and  $[6 \cdot (n - 2) + 8 \cdot n - 12]$  six-DOF relative position sensors. A preliminary assessment of controllability in progress, based on a baseline optical model of an array constructed using the principles described in preceding sections. The control assessment will also require knowledge of mechanical distortion and vibration, which is also in progress, described briefly in section §3.

## 3. MECHANICAL ANALYSIS

### 3.1. Structural Modes and Optical Alignment

A 3-D model was created for a three-element emitter, shown in Fig. 9. The model is based on individual hexagonal emitter cells, which are shown in Fig. 3 and Fig. 4.

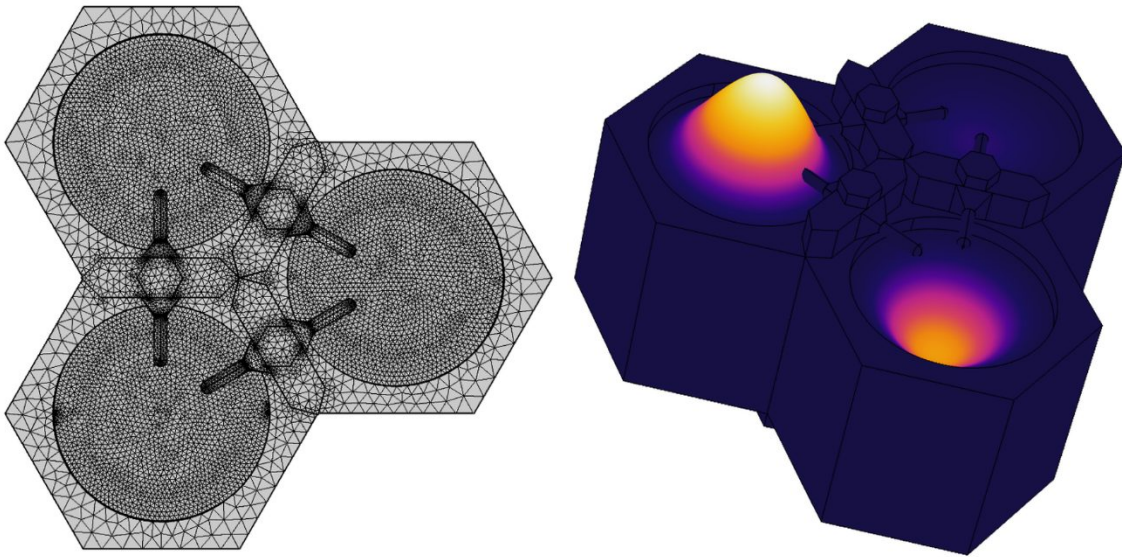


**Figure 9. Left:** Meshed 3-element emitter, with thin-film lenses. **Right:** The third Eigenmode of the structure, showing resonant oscillations between adjacent lens elements. The simulation was performed with thin-film holographic lens elements. Magnitude of the oscillations is shown exaggerated; displacement of the lens elements would result in significant phase misalignment and beam degradation.

## 4. CONCLUSIONS

Current laser phased array designs rely on an array-wide beamsplitter for phase feedback and phase control. In a scenario where an emitter cell is to be added to an existing emitter array, the beamsplitter would need to be replaced, and an array-wide control system recalibration would be required. As such, existing laser phased array designs are not so easily extensible. A conceptual design and phase control scheme is offered that is modular and extensible without requiring beamsplitter replacement or full-array re-calibrations. The technology would be useful if an array were to be constructed in stages, such as in low-Earth orbit. The basic concept for phase control is to align phases of all emitters in a reference plane that is normal to the target vector. A resultant target vector is determined from the combined information of all individual target sensors in the array, and within a common global coordinate system. The spatial relationship between adjacent target sensors is determined by 6-DOF position sensors, and the relative positioning is used to establish the global coordinate system. The position of target sensors and phase tap structures within the global coordinate system is determinable in control-time. Phase feedback is determined by the distance of each phase tap from the reference plane. Controllability of an array is being investigated, beginning with optical models that incorporate realistic sources of phase perturbations for individual emitters.

A design and method for a fast, 6-DOF relative position sensor are described. The sensor is based on active triangulation laser measurements, and is suitable for applications where the relative position of two fixed, rigid mechanical components is to be measured dynamically with high precision. The method uses an array of several laser emitters mounted on one component, which are directed at a reflective surface on the second component. The reflective surface is curved; examples are described using a pyramid and a hyperbolic paraboloid. The reflected spots are sensed at 2-dimensional photodiode arrays on the emitter component. Changes in the relative position of the emitter component and reflective surface shift the location of the reflected spots within photodiode arrays. Relative motion in any degree of freedom produces independent shifts in the reflected spot locations, allowing full six-DOF relative position determination between the two component positions. Response time of the sensor is limited by the read-out rate of the photodiode arrays. Position is determined using constrained optimization, and can be implemented in FPGA. Limits on relative position uncertainty and sensitivity are achievable, based on laser and spot-sensor characteristics, and assuming regular surfaces. Continuing work will address uncertainty analysis, including deviations due to surface irregularities. The sensor is being developed to support a system with multiple target acquisition sensors. As the sensors must be mounted within a mechanical structure subject to vibration. The sensors are envisioned to make control-time measurements of the relative position of sensor housings within a local mechanical datum coordinate system, thus improving the target vector from the sensing structure.

## ACKNOWLEDGEMENTS

We gratefully acknowledge funding from the NASA California Space Grant NASA NNX10AT93H in support of this research. We also gratefully acknowledge funding from the NASA Innovative Advanced Concepts grant NNX16AK30G in support of this research.

## REFERENCES

- [1] Lubin, P., Hughes, G.B., Bible, J., Publitz, J., Arriola, J., Motta, C., Suen, J., Johansson, I., Riley, J., Sarvian, N., Clayton-Warwick, D., Wu, J., Milich, A., Oleson, M., Pryor, M., Krogen, P., Kangas, M., and O'Neill, H. "Toward Directed Energy Planetary Defense," *Optical Engineering*, 53(2), pp 025103-025103 (2014).
- [2] Lubin, P., Hughes, G.B., Eskenazi, M., Kosmo, K., Johansson, I., Griswold, J., Pryor, M., O'Neill, H., Meinhold, P., Suen, J., Riley, J., Zhang, Q., Walsh, K.J., Melis, C., Kangas, M., Motta, C. and Brashears, T. "Directed Energy Missions for Planetary Defense," *Advances in Space Research*, 58(6), pp. 1093–1116 (2016).
- [3] Zhang, Q., Walsh, K.J., Melis, C., Hughes, G.B. and Lubin, P.M. "Orbital Simulations on Deflecting Near Earth Objects by Directed Energy," *Publications of the Astronomical Society of the Pacific*, 128(962), pp. 045001 (2016).

- [4] Lubin, P., Hughes, G.B., Bible, J., Bublitz, J., Arriola, J., Motta, C., Suen, J., Johansson, I., Riley, J., Sarvian, N., Clayton-Warwick, D., Wu, J., Milich, A., Oleson, M., Pryor, M., Krogan, P. and Kangas, M. "Directed energy planetary defense," *Nanophotonics and Macrophotonics for Space Environments VII*, edited by Edward W. Taylor, David A. Cardimona, Proc. of SPIE Vol. 8876, pp. 887602 (2013).
- [5] Hughes, G.B., Lubin, P., Bible, J., Bublitz, J., Arriola, J., Motta, C., Suen, J., Johansson, I.E., Riley, J., Sarvian, N., Wu, J., Milich, A., Oleson, M., and Pryor, M. "DE-STAR: phased-array laser technology for planetary defense and other scientific purposes," *Nanophotonics and Macrophotonics for Space Environments VII*, edited by Edward W. Taylor, David A. Cardimona, Proc. of SPIE, Vol. 8876, 88760J (2013).
- [6] Kosmo, K., Lubin, P., Hughes, G.B., Griswold, J., Zhang, Q. and Brashears, T. "Directed Energy Planetary Defense," *Aerospace Conference 2015 IEEE Proceedings*, pp. 1-9 (2015).
- [7] Kosmo, K., Pryor, M., Lubin, P., Hughes, G.B., O'Neill, H., Meinhold, P., Suen, J., C., Riley, J., Griswold, J., Cook, B.V., Johansson, I.E., Zhang, Q., Walsh, K., Melis, C., Kangas, M., Bible, J., Motta, Brashears, T., Mathew, S. and Bollag, J. "DE-STARLITE - a practical planetary defense mission," *Nanophotonics and Macrophotonics for Space Environments VIII*, edited by Edward W. Taylor, David A. Cardimona, Proc. of SPIE, Vol. 9226 (2014).
- [8] Hughes, G.B., Lubin, P., Meinhold, P., O'Neill, Brashears, T., Zhang, Q., Griswold, J., Riley, J., and Motta, C. "Stand-off molecular composition analysis," *Nanophotonics and Macrophotonics for Space Environments IX*, edited by Edward W. Taylor, David A. Cardimona, Proc. of SPIE, Vol. 9616, pp. 961603-961603 (2015).
- [9] Riley, J., Lubin, P., Hughes, G.B., O'Neill, H., Meinhold, P., Suen, J., Bible, J., Johansson, I.E., Griswold, J. and Cook, B. "Directed energy active illumination for near-Earth object detection," *Nanophotonics and Macrophotonics for Space Environments VIII*, edited by Edward W. Taylor, David A. Cardimona, Proc. of SPIE Vol. 9226 (2014).
- [10] Lubin, P., Hughes, G.B., Bible, J. and Johansson, I. "Directed Energy for Planetary Defense and Exploration: Applications to Relativistic Propulsion and Interstellar Communications," *Journal of the British Interplanetary Society*, 68(5/6), pp. 172-182 (2015).
- [11] Bible, J., Bublitz, J., Johansson, I.E., Hughes, G.B., and Lubin, P. "Relativistic Propulsion Using Directed Energy," *Nanophotonics and Macrophotonics for Space Environments VII*, edited by Edward W. Taylor, David A. Cardimona, Proc. of SPIE Vol. 8876, pp. 887605 (2013).

#### **Fiber Laser Amplifiers and Laser Phased Arrays**

- [12] Zervas, M.N. and Codemard, C.A. "High power fiber lasers: a review." *IEEE Journal of Selected Topics in Quantum Electronics*, vol. 20, no. 5, pp. 219-241 (2014).
- [13] Wagner, T.J. "Fiber laser beam combining and power scaling progress: Air Force Research Laboratory Laser Division." *SPIE LASE*, pp. 823718-823718. Proc. of SPIE vol. 8237 (Feb, 2012).
- [14] Vorontsov, M.A., Weyrauch, T., Beresnev, L.A., Carhart, G.W., Liu, L. and Aschenback, K. "Adaptive Array of Phase-Locked Fiber Collimators: Analysis and Experimental Demonstration," *IEEE Journal of Selected Topics in Quantum Electronics*, vol. 15, 269 (2009).
- [15] Liu, H., He, B., Zhou, J., Dong, J., Wei, Y., & Lou, Q. "Coherent beam combination of two nanosecond fiber amplifiers by an all-optical feedback loop." *Optics Letters*, 37(18), 3885-3887 (2012).
- [16] Su, R., Zhou, P., Wang, X., Zhang, H., & Xu, X. "Active coherent beam combining of a five-element, 800 W nanosecond fiber amplifier array." *Optics Letters*, 37(19), 3978-3980 (2012)
- [17] Yu, C.X., Augst, S.J., Redmond, S.M., Goldizen, K.C., Murphy, D.V., Sanchez, A., and Fan, T.Y. "Coherent combining of a 4 kW, eight-element fiber amplifier array." *Optics Letters*, 36(14), 2686-2688 (2011).

#### **SPGD Control of Laser Phased Arrays**

- [18] Vorontsov, M., Carhart, G.W. and Ricklin, J.C. "Adaptive Phase Distortion Correction Based On Parallel Gradient Descent Optimization," *Optics Letters*, 22(12), pp. 907-909 (1997).
- [19] Liu, L., Vorontsov, M.A., Polnau, E., Weyrauch, T. and Beresnev, L.A. "Adaptive Phase-Locked Fiber Array with Wavefront Phase Tip-Tilt Compensation using Piezoelectric Fiber Positioners," in: *Atmospheric Optics: Models, Measurements, and Target-in-the-Loop Propagation*, edited by Stephen M. Hammel, Alexander M. J. van Eijk, Michael T. Valley, Mikhail A. Vorontsov, Proc. of SPIE, Vol. 6708, pgs. 67080K-1 – 67080K-12 (2007).
- [20] Zhou, P., Liu, Z., Wang, X., Ma, Y., Ma, H. and Xu, X. "Coherent Beam Combination of Two Dimensional High Power Fiber Amplifier Array Using Stochastic Parallel Gradient Descent Algorithm." *Applied Physics Letters*, Vol. 94, No. 231106, pgs. 231106-1 – 231106-3 (2009).

- [21] Zhou, P., Liu, Z., Wang, X., Ma, Y., Ma, H., and Xu, X. "Coherent Beam Combining of Two Fiber Amplifiers Using Stochastic Parallel Gradient Descent Algorithm." *Optics & Laser Technology*, Vol. 41, pp. 853 – 856 (2009).

#### **Optical Modeling and Dynamic Metrology**

- [22] Hughes, G.B., Macasaet, V.P., Griswold, J., Sison, C.A., Lubin, P., Meinhold, P., Suen, J., Brashears, T., Zhang, Q. and Madajian, J. "A fast, high-precision six-degree-of-freedom relative position sensor," *Photonic Instrumentation Engineering III*, edited by Yakov G. Soskind and Craig Olson, Proc. Of SPIE Vol. 9754, pp. 975403-975403 (2016).
- [23] Hughes, G.B., Lubin, P., Griswold, J., Bozinni, D., O'Neill, H., Meinhold, P., Suen, J., Bible, J., Riley, J., Johansson, I., Pryor, M. and Kangas, M. "Optical modeling for a laser phased-array directed energy system," *Nanophotonics and Macrophotonics for Space Environments VIII*, edited by Edward W. Taylor, David A. Cardimona, Proc. of SPIE Vol. 9226, pp. 922603 (2014).
- [24] Chugui, Y.V. "Three-dimensional optoelectronic measurement systems and laser technologies for scientific and industrial applications," *Optoelectronics, Instrumentation and Data Processing*, 51(4), 385-397 (2015).
- [25] Chugui, Y.V., Verkhogliad, A., Kalikin, V., and Zav'yalov, P. "3D optical measuring technologies for industrial applications," *Optical Measurement Systems for Industrial Inspection VII*, edited by Peter H. Lehmann, Wolfgang Osten, Kay Gasteringer, Proc. of SPIE Vol. 8082, 808222 (2011).
- [26] Chugui, Y.V., Verkhoglyad, A., Poleshchuk, A., Korolkov, V., Sysoev, E., and Zavyalov, P. "3D Optical Measuring Systems and Laser Technologies for Scientific and Industrial Applications," *Measurement Science Review*, 13(6), 322-328 (2013).
- [27] Chugui, Y.V., Bazin, V.S., Finogenov, L.V., Makarov, S.N., and Verkhogliad, A.G. "Optical electronic measuring systems and laser technologies for scientific and industrial applications," *Sixth International Symposium on Instrumentation and Control Technology: Signal Analysis, Measurement Theory, Photo-Electronic technology, and Artificial Intelligence*, edited by Jiancheng Fang, Zhongyu Wang, Proc. of SPIE Vol. 6357, 63571T (2006).
- [28] Schwenke, H., Neuschaefer-Rube, U., Pfeifer, T., and Kunzmann, H. "Optical methods for dimensional metrology in production engineering," *CIRP Annals-Manufacturing Technology*, 51(2), 685-699 (2002).
- [29] Garcia, E., Hausotte, T., and Amthor, A. "Bayes filter for dynamic coordinate measurements – Accuracy improvement, data fusion and measurement uncertainty evaluation," *Measurement*, 46, 3737–3744 (2013).
- [30] Hessling, J.P. "Propagation of dynamic measurement uncertainty," *Measurement Science and Technology*, 22(10), 105105 (2011).
- [31] Hessling, J.P. "A novel method of evaluating dynamic measurement uncertainty utilizing digital filters," *Measurement Science and Technology*, 20(5), 055106 (2009).
- [32] Hessling, J.P. "Dynamic metrology—an approach to dynamic evaluation of linear time-invariant measurement systems," *Measurement Science and Technology*, 19(8), 084008 (2008).
- [33] Hessling, J.P. "A novel method of estimating dynamic measurement errors," *Measurement Science and Technology*, 17, 2740-2750 (2006).
- [34] Elster C., and Link A. "Uncertainty evaluation for dynamic measurements modelled by a linear time-invariant system," *Metrologia*, 45, 464-473 (2008).
- [35] Vasilevskyi, O. M., Kucheruk, V. Y., and Kurytnik, I. P. "An approach to the evaluation of dynamic uncertainty in measurement using non-statistical techniques," *PAK*, 60(11), 997-1001 (2014).
- [36] Vasilevskyi, O. M. "A frequency method for dynamic uncertainty evaluation of measurement during modes of dynamic operation," *International Journal of Metrology and Quality Engineering*, 6(2), 202 (2015).
- [37] D'Errico, G.E., and Murru, N. "Real-time estimation of dynamic-multidimensional measurands," *Proceedings of the XX IMEKO World Congress, Metrology for green growth, Busan, Republic of Korea*, (2012).
- [38] D'Errico G.E., and Murru, N. "An algorithm for concurrent estimation of time-variant quantities," *Measurement Science and Technology*, 23(4), 045008 (2012).
- [39] Beraldin, J.A., Blais, F., Rioux, M., Domey, J., Gonzo, L., De Nisi, F., Comper, F., Stoppa, D., Gottardi, M. and Simoni, A. "Optimized position sensors for flying-spot active triangulation systems," *Proceedings of the Fourth International Conference on 3-D Digital Imaging and Modeling (3DIM)*, NRC 47083, 334-341 (2003).
- [40] Beraldin, J. A., and Gaiani, M. "Evaluating the performance of close-range 3D active vision systems for industrial design applications," *Electronic Imaging, Proceedings of SPIE 5665*, 67-77 (2005).
- [41] Isheil, A., Gonnet, J.P., Joannic, D., and Fontaine, J.F. "Systematic error correction of a 3D laser scanning measurement device," *Optics and Lasers in Engineering*, 49(1), 16-24 (2011).

- [42] English, C., Zhu, S., Smith, C., Ruel, S., and Christie, I. "Tridar: A hybrid sensor for exploiting the complimentary nature of triangulation and LIDAR technologies, Proceedings of the 8th International Symposium on Artificial Intelligence, Robotics and Automation in Space, ESA SP-603 (2005).
- [43] English, C., Okouneva, G., Saint-Cyr, P., Choudhuri, A., and Luu, T. "Real-time dynamic pose estimation systems in space: lessons learned for system design and performance evaluation," *International Journal of Intelligent Control and Systems*, 16(2), 79-96 (2011).
- [44] Deb, S., Yeddanapudi, M., Pattipati, K., and Bar-Shalom, Y. "A generalized SD assignment algorithm for multisensor-multitarget state estimation," *IEEE Transactions on Aerospace and Electronic Systems*, 33(2), 523-538 (1997).
- [45] Weckenmann, A., Jiang, X., Sommer, K.D., Neuschaefer-Rube, U., Seewig, J., Shaw, L., and Estler, T. "Multisensor data fusion in dimensional metrology," *CIRP Annals-Manufacturing Technology*, 58(2), 701-721 (2009).
- [46] Sun, S.L., and Deng, Z.L. "Multi-sensor optimal information fusion Kalman filter," *Automatica*, 40(6), 1017-1023 (2004).
- [47] Sun, S.L. "Multi-sensor optimal information fusion Kalman filters with applications," *Aerospace Science and Technology*, 8(1), 57-62 (2004).
- [48] Xiong, N., and Svensson, P. "Multi-sensor management for information fusion: issues and approaches," *Information fusion*, 3(2), 163-186 (2002).
- [49] Khaleghi, B., Khamis, A., Karray, F.O., and Razavi, S.N. "Multisensor data fusion: A review of the state-of-the-art," *Information Fusion*, 14(1), 28-44 (2013).
- [50] Hughes, G.B. "Algorithms for sensor chip alignment to blind datums," *Journal of Electronic Imaging*, 15(3), 033003 (2006).
- [51] Lubin, P., Hughes, G.B., Bible, J., Bublitz, J., Arriola, J., Motta, C., Suen, J., Johansson, I., Riley, J., Sarvian, N., Clayton-Warwick, D., Wu, J., Milich, A., Oleson, M., Pryor, M., Krogen, P., Kangas, M., and O'Neill, H. "Toward directed energy planetary defense," *Optical Engineering*, 53(2), 025103 (2014).
- [52] Steffanic, P., Johannes, B.T., Sison, C.A., Hughes, G.B., Lubin, P., Meinhold, P., Suen, J., O'Neill, H., Kangas, M., Brashears, T., Zhang, Q., Griswold, J., Riley, J., and Motta, C. "Local phase control for a planar array of fiber laser amplifiers," *Nanophotonics and Macrophotonics for Space Environments IX*, edited by Edward W. Taylor, David A. Cardimona, Proc. of SPIE, 9616 (2015).
- [53] Tsai, R.Y. "A versatile camera calibration technique for 3D machine vision metrology using off-the-shelf TV cameras and lenses," *IEEE Journal of Robotics & Automation*, RA-3(4), 323-344 (1987).
- [54] Zhang, Z. "A flexible new technique for camera calibration," *IEEE Transactions on Pattern Analysis and Machine Intelligence*, 22(11), 1330-1334 (2000).
- [55] Sun, Q., Hou, Y., Tan, Q., and Li, G. "A flexible calibration method using the planar target with a square pattern for line structured light vision system," *PLOS One*, 9(9), e106911 (2014).
- [56] Kannala, J., and Brandt, S.S. "A generic camera model and calibration method for conventional, wide-angle, and fish-eye lenses," *IEEE Transactions on Pattern Analysis and Machine Intelligence*, 28(8), 1335-1340 (2006).